



CHORUS

This is the accepted manuscript made available via CHORUS. The article has been published as:

Plasmonic Resonant Intercluster Coulombic Decay

Rasheed Shaik, Hari R. Varma, Mohamed El-Amine Madjet, Fulu Zheng, Thomas Frauenheim, and Himadri S. Chakraborty

Phys. Rev. Lett. **130**, 233201 — Published 7 June 2023

DOI: [10.1103/PhysRevLett.130.233201](https://doi.org/10.1103/PhysRevLett.130.233201)

Plasmonic Resonant Intercluster Coulombic Decay

Rasheed Shaik,¹ Hari R. Varma,^{1,*} Mohamed El-Amine Madjet,^{2,3}
Fulu Zheng,² Thomas Frauenheim,^{2,4,5} and Himadri S. Chakraborty^{3,†}

¹*School of Physical Sciences, Indian Institute of Technology Mandi, Kamand, H.P. 175075, India*

²*Bremen Center for Computational Materials Science, University of Bremen, Bremen, Germany*

³*Department of Natural Sciences, D.L. Hubbard Center for Innovation,*

Northwest Missouri State University, Maryville, Missouri 64468, USA

⁴*Beijing Computational Science Research Center, 100193 Beijing, China*

⁵*Shenzhen JL Computational Science and Applied Research Institute, 518110 Shenzhen, China*

Light-induced energy confinement in nanoclusters via plasmon excitations influences applications in nanophotonics, photocatalysis, and the design of controlled slow electron sources. The resonant decay of these excitations through the cluster's ionization continuum provides a unique probe of the collective electronic behavior. However, the transfer of a part of this decay amplitude to the continuum of a second conjugated cluster may offer control and efficacy in sharing the energy nonlocally to instigate remote collective events. With the example of a spherically nested dimer $\text{Na}_{20}@\text{C}_{240}$ of two plasmonic systems we find that such a transfer is possible through the resonant intercluster Coulombic decay (RICD) as a fundamental process. This plasmonic RICD signal can be experimentally detected by the photoelectron velocity map imaging technique.

Resonant (electronic) energy transfer (RET), first observed a century ago [1], is mediated by virtual photon exchange between weakly bonded sites embedded in chemical or biological environments [2]. The donor and the acceptor in this process are coupled by the quantum electrodynamic dipole interaction. Particularly fascinating are the RET processes *mediated* by the plasmon [3, 4], the collective excitation of conduction electrons. However, RET is confined in the excitations of the upper-lying electron levels that occurs within the visible to mid-ultraviolet electromagnetic spectrum.

A very different class of processes emerges when the absorbed photon is within the range of extreme ultraviolet (XUV) to x-ray. This photon can energetically access both the innershell excitation in the donor and the outershell ionization in the acceptor. The innershell vacancy can then *resonantly* decay through the acceptor's ionization continuum with the Coulomb interaction between the degenerate excitation and the ionization channel being the mediator. Such resonant, and other non-resonantly relaxing, interatomic and intermolecular Coulombic decay (ICD) processes have been the subject of a vast range of studies [5] since the effect's discovery by Cederbaum and collaborators [6] more than two decades ago. In one original experiment, the precursor excitation was induced in Ne dimers by the synchrotron radiation [7]. Later for higher pulse rates to carry out time-resolved measurements, free electron laser (FEL) sources are found appropriate [8]. ICD signatures are also probed by electron [9, 10] and ion [11] spectroscopy. These include various coincidence techniques, namely, the velocity map imaging (VMI) technique [12]. Contemporary pump-probe approaches [8, 13], specifically by light field streaking techniques [14], to access time-resolved ICD are also made possible. Recently, the measurement of ICD in liquid water [15] and ICD-based transfer of ex-

cess energy to the surroundings of water at nanoplatelet interfaces [16] are reported. A fascinating control of ICD in the cavity of quantum light [17] is published, while ICD electrons for unbound (gaseous) system of pyridine monomers based on the energy-transfer through associative interactions has been measured [18].

The fundamental process that underpins the swath of current ICD landscape is the decay of an innershell vacancy. The other is a resonantly enhanced multi-photon absorption by FEL, leading to a multiple-vacancy state occurring prior to the formation of a plasmon. This subsequently decays in a collective autoionization [19]. The ICD relaxation of such multiply excited states in neon clusters is measured to be very slow as in picoseconds [20].

Remarkably, no evidence of the decay of a plasmon resonance through an ICD channel is yet found. However, owing to characteristic extreme light confinement and control abilities within the nanoscale size, the plasmonic ICD will not only be a fundamental process, but also can substantially enrich the scopes within the vast ICD landscape and related applications in physics, chemistry, and biology. For instance, possibility and control of plasmon-driven remote-photonics, remote-catalysis or even remote-release of secondary electrons can be within the technological reach. With this motivation, we found an efficient prototype system in the nanocluster $\text{Na}_{20}@\text{C}_{240}$ to probe the *intercluster* Coulombic decay of a plasmon excitation and revealed the first evidence of this fundamental phenomenon.

Structure studies [21] of $\text{Na}_{20}@\text{C}_{240}$ and a review [22] on clusterfullerenes are available. $\text{Na}_{20}@\text{C}_{240}$ is a spherical compound of a sodium sub-nano particle endohedrally confined in a carbon fullerene forming a nanometric spherical dimer. Both the units support their intrinsic (native) plasmon excitations. The plasmon of Na_{20} excites in the visible spectrum below its first ionization

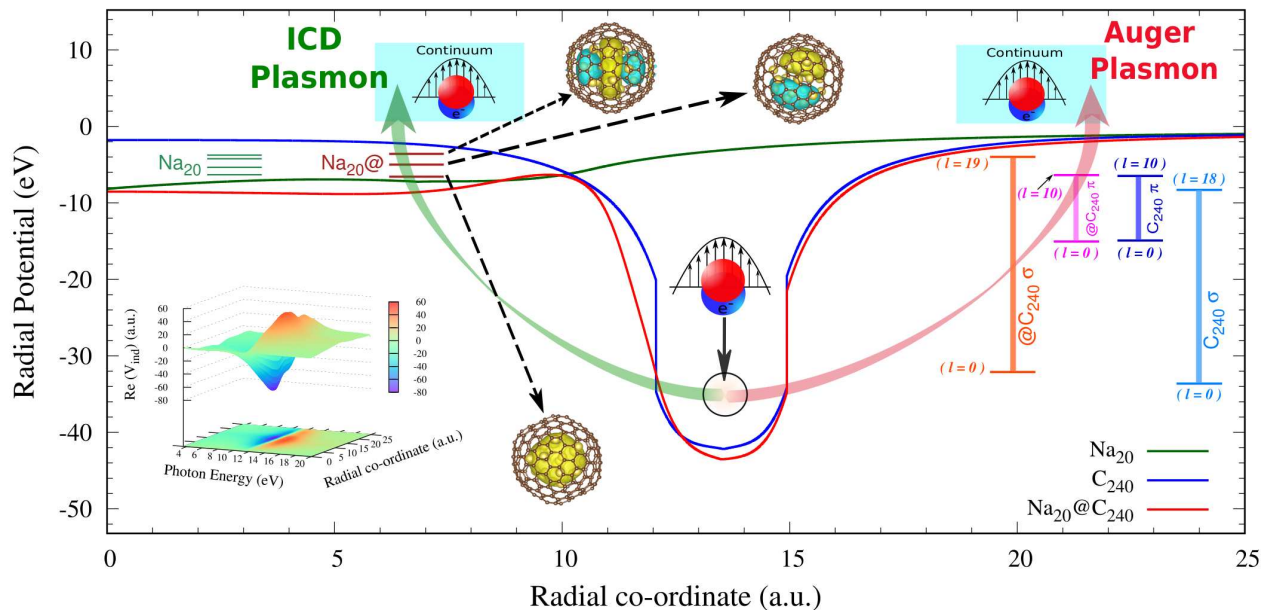


FIG. 1. (Color online) A cartoon to delineate the process of resonant Auger and ICD plasmon decays in $\text{Na}_{20}@C_{240}$, with curved arrows mimicking these decays [Eq. (2)]. The ground state DFT radial potentials of $\text{Na}_{20}@C_{240}$, isolated Na_{20} , and empty C_{240} are drawn (solid curves). The corresponding Na_{20} occupied energy levels as well as C_{240} π and σ occupied band edges, defined by the maximum and minimum angular quantum number (l), are shown; among the levels of $\text{Na}_{20}@C_{240}$, the symbols $\text{Na}_{20}@$ and $@C_{240}$ are used to distinguish from free system levels. The isosurface orbitals (HOMO, HOMO-6, HOMO-23) from quantum chemical calculations representing the three $\text{Na}_{20}@$ states are shown. Inset: The real part of the LR-TDDFT induced radial potential (V_{ind}) for $\text{Na}_{20}@C_{240}$.

threshold in the absorption response [23, 24], while the giant plasmon (GP) excitation of C_{240} embeds in the ionization continuum at the XUV spectral region, similar to the well known GP of C_{60} . Being energetically so separated, the hybridization [25] of these native plasmons is forbidden in $\text{Na}_{20}@C_{240}$ ensuring reliability of the current result. Incidentally, C_{60} with confined atoms is studied for variants of ICD processes [26–30], but for ordinary single-electron vacancy decay resonances. A recent experiment to measure the ICD relaxation between the holmium nitride molecule and its C_{80} cage has been reported [31].

The details of the computational methodology are given as supplementary materials (SM) [32]. The ground states ($1s^21p^61d^{10}2s^2$ in the harmonic oscillator notation) of the free Na_{20} cluster, the empty C_{240} molecule, and the endofullerene $\text{Na}_{20}@C_{240}$ are modeled by a jellium-based density functional theory (DFT) in the spherical frame. The DFT ground configuration of $\text{Na}_{20}@C_{240}$ well replicates our detailed quantum chemical (QC) calculations [32] providing significant accuracy of the ground state description. This entailed the transfer of six Na_{20} electrons to the fullerene shell leaving fourteen valence delocalized electrons ($1s^21p^61d^6$) in the cluster. The DFT radial potentials are plotted in Figure 1 along with the corresponding electronic energy-levels. As seen, the three Na_{20} levels denoted by $\text{Na}_{20}@$ slightly shift in

the compound; for details, see Figure S1 in SM [32]. Remarkably, the d , p , and s -type angular momentum character of these delocalized DFT $\text{Na}_{20}@$ levels are almost exactly reproduced by our simulated QC orbitals as shown. The fullerene bands of the π (the group of one radial node) and σ (the group of no radial node) states are identified in Fig. 1 with band edges defined by the angular quantum number (l). The π band exhibits stronger energy-stability with ($@C_{240}$) or without (C_{240}) Na_{20} .

The dipole response of the systems to the incoming photon is described and computed by a linear response time-dependent DFT (LR-TDDFT) approach [38, 39], since it is extremely challenging to use the QC framework to describe the electron continuum. The current approach has a track record of success in explaining measurements of (i) plasmonic photodepletion spectra [23, 24] and (ii) photoelectron [46] and photoion [47] intensity, respectively, at non-plasmonic and plasmonic energies. LR-TDDFT encodes the electron many-body correlations in the calculated induced potential, which is a complex quantity [32]. The large-scale coherent component of the correlation over the GP formation energies blocks (screens) the incoming radiation but allows (anti-screens) the radiation to couple to the electrons at energies above the GP peak ~ 11.5 eV. This shape reversal is seen in Fig. 1 (inset) in the real part of the induced radial potential for $\text{Na}_{20}@C_{240}$ over the C_{240} shell region that

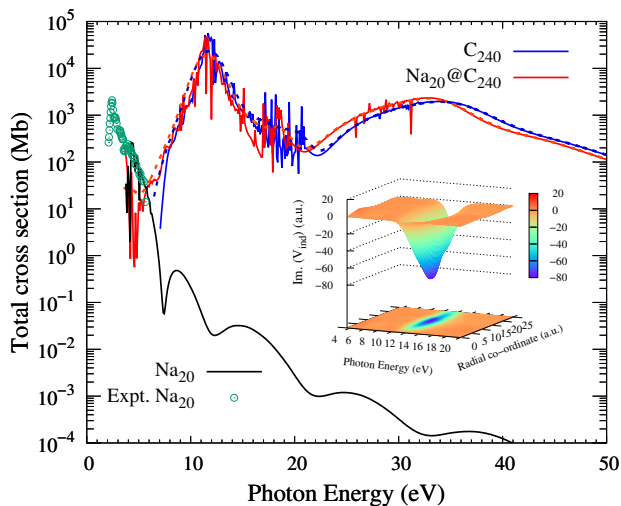


FIG. 2. LR-TDDFT total photoionization cross sections for C_{240} , $Na_{20}@C_{240}$ and Na_{20} . Smoothed curves are added to guide the eye for the fullerene systems. The experimental absorption data [23] are included for Na_{20} . Inset: The imaginary part of the induced radial potential (V_{ind}) for $Na_{20}@C_{240}$ calculated in LR-TDDFT.

sluices through a zero at the GP peak energy.

An elegant way to visualize the plasmon formation is to consider, in terms of many-body ground $|\Phi_0\rangle$ and excited collective $|\Phi_m\rangle$ states, the complex polarizability α from electrons' interactions with the photon of frequency ω [48]. Using the Fermi's Golden rule, the absorption cross section σ relates to the imaginary part of α as [49]

$$\begin{aligned} \sigma(\omega) &\sim \text{Im}[\alpha(\omega)] \\ &\sim \sum_m \left[\frac{|\langle \Phi_m | \zeta | \Phi_0 \rangle|^2}{[\hbar\omega - \Delta_m]^2 + \delta^2} - \frac{|\langle \Phi_m | \zeta | \Phi_0 \rangle|^2}{[\hbar\omega + \Delta_m]^2 + \delta^2} \right] \end{aligned} \quad (1)$$

where $\zeta = \sum_i z_i$ are dipole interactions, $\Delta_m = E_m - E_0$ are many-body excitation energies, and δ is an infinitesimal positive quantity. Eq. (1) embodies the notion that the plasmons at photon energies Δ_m are due to excitations of the ground state Φ_0 to all possible collective excited states Φ_m that the system supports.

Both the GP and a much weaker high-energy plasmon (HP) excitations of C_{240} energetically embed in the system's ionization continuum. Thus, they produce GP resonance (GPR) and HPR in LR-TDDFT photoionization cross sections, as seen in Figure 2, both for C_{240} and $Na_{20}@C_{240}$. The narrow structures represent the incoherent single electron inner-shell excitation resonances and are not relevant for the current study. An attractive-shaped imaginary part of the induced radial potential of $Na_{20}@C_{240}$ (inset of Fig. 2), dipping at the GP peak and locating across the C_{240} shell, transiently binds the collective excitation. An excellent agreement of the current theory with recent pump-probe streaking measurements accesses the resulting photoemission time delay at GP

in C_{60} [50]. Both the plasmon resonances in C_{240} can therefore be visualized as the decays through C_{240} continuum emissions following the de-excitations of the plasmon states. In this spirit, they can be called the *Auger* plasmon resonances (Fig. 1). The free Na_{20} photoionization spectrum over this XUV energy range is very weak and completely plasmon-barren (Fig. 2). In fact, Na_{20} 's native plasmon excites at a far lower 2 eV photon energy as seen in the measured data [23]; note also the agreement of the data at higher energies with the trend of the Na_{20} cross section. Furthermore, the real (Fig. 1) and the imaginary (Fig. 2) parts of the induced radial potential are featureless over the central Na_{20} region of the compound. Yet, our current results exhibit a plasmon-like resonance in the $Na_{20}@$ ionization channel which exhausts comparable oscillator strength (OS) used by the native plasmon resonance of Na_{20} (see Figure 4). This must be the resonant ICD (RICD) transfer of the C_{240} GP as schematically shown in Fig. 1. The process is resonant, since the GP excitation energy inlays the Na_{20} ionization continuum. As the precursor plasmon excitation itself decays, the process qualifies for a participant RICD. The ICD transfer from HP is, however, negligibly weak and will be disregarded.

A framework to understand this RICD transfer can be modeled upon the well-known discrete-continuum interchannel-coupling approach by Fano [51]. The RICD amplitude of the C_{240} plasmon "vacancy"-decay *via* the Na_{20} $nl@$ ionization can be expressed by M^{P-c} . This will include the coupling of C_{240} $0 \rightarrow m$ plasmon (p) excitation channel with the $nl@ \rightarrow kl'$ continuum (c) channel of Na_{20} . Hence, M^{P-c} can be written as:

$$\begin{aligned} M_{nl@}^{P-c}(E) &\sim \frac{\langle 0 \rightarrow m | \frac{1}{|\mathbf{r}_p - \mathbf{r}_{nl@}|} | nl@ \rightarrow kl'(E) \rangle}{E - \Delta_m} \mathcal{D}_{0 \rightarrow m}(2) \end{aligned}$$

where $\mathcal{D}_{0 \rightarrow m}$ is the plasmonic amplitude of $@C_{240}$ photoionization and E is the photon energy that enables the Na_{20} $nl@$ transition to the continuum. By motivating \mathbf{r}_p to be the "co-ordinate" of the plasmon quasi-particle, the Coulomb-type coupling matrix element in the numerator of Eq. (2) acts as the passage for virtual energy-transfer from the GP de-excitation across to the Na_{20} ionization, producing plasmonic ICD resonances in a Na_{20} $nl@$ cross section. In effect, a conduit of this passage is the overlap between the wave functions involving the collective excitation and the Na_{20} ionization channels in the Coulomb matrix element.

We capture the RICD signals in the $Na_{20}@$ channels by generating iso-contour images of cross section as a function of photon energy and photoelectron kinetic energy in Figure 3. Such images can be produced in the experiment by using the standard VMI coincidence technique [52] to separate and selectively detect photoions or photoelectrons by mass and velocity. Here we used

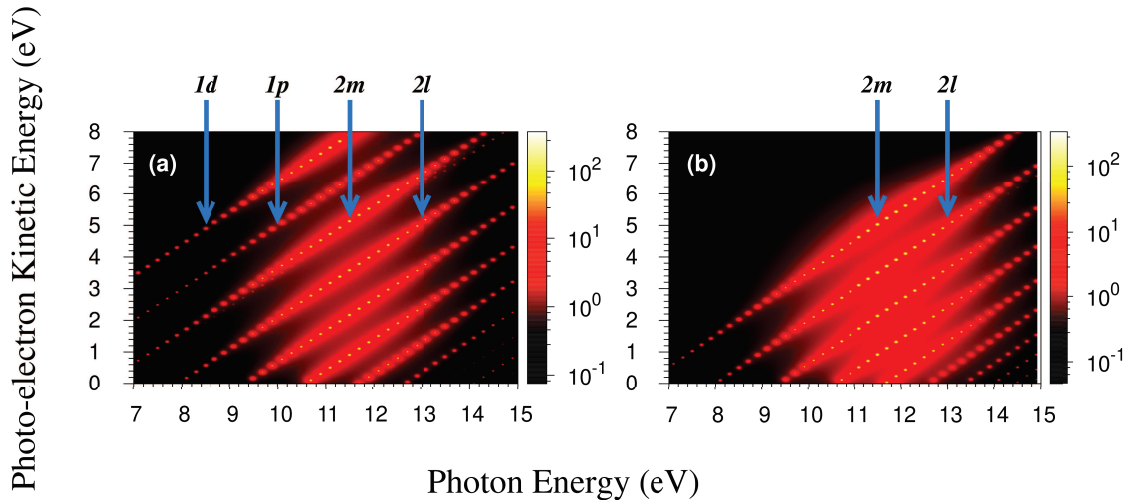


FIG. 3. (Color online) Color coded cross section maps as a function of photon energy and photoelectron kinetic energy for $\text{Na}_{20}@\text{C}_{240}$ (a) and C_{240} (b). The smoothed curves are used to solely capture the plasmon resonance signals and some blur is introduced to highlight the resonance profiles. Plasmonic RICD traces from $1d$ and $1p$ $\text{Na}_{20}@\text{C}_{240}$ levels are identified in panel (a) ($1s$ is too weak to show in this scale), while both panels show similar distributions of regular Auger plasmon traces in C_{240} levels within the range shown. Auger traces in both (a) and (b) are somewhat scaled down for better contrast.

the cross sections after smoothing the profiles for narrow resonance spikes in order to feature only the broad plasmonic contributions. The vertical sections of the images provide the photoelectron energy distribution of the signal by mapping the ionization thresholds of the levels. The subshell cross sections as a function of the photon energy can be extracted from horizontal sections. Comparing Fig. 3(a) for $\text{Na}_{20}@\text{C}_{240}$ with Fig. 3(b) for C_{240} , the additional traces seen in the former are, obviously, the Na_{20} RICD signals, while the C_{240} Auger signals are common in both panels. Note, as expected, that all the traces peak within 11–12 eV photon energy range.

Fig. 4(a) displays the total (smoothed) cross sections of $\text{Na}_{20}@\text{C}_{240}$ and C_{240} . The curves are fitted with two Lorentzian profiles, accounting the two plasmon resonances; the values of the fitting parameters for GPR are tabulated. The peak energy (E_0) is found to slightly red-shift when Na_{20} is present. The corresponding increase in the resonance line-width (Γ) from 2.12 eV to 2.18 eV amounts to somewhat shortening of the lifetime from 610 attoseconds (as) to 595 as. Going from C_{240} to $\text{Na}_{20}@\text{C}_{240}$, this effect must be due to the additional (ICD) decay rate introduced by the Na_{20} ionization channels. The ICD contribution is shown independently as $\text{Na}_{20}@\text{C}_{240}$ in Fig. 4(b). This RICD plasmon feature yields a narrower line-width of 2.07 eV corresponding to a longer lifetime of about 625 as. The implication is that the average dephasing of the RICD feature is slower than the resonant Auger feature – a fact which may benefit time domain measurements to separate and probe the plasmonic ICD. The difference between $\text{Na}_{20}@\text{C}_{240}$ and C_{240}

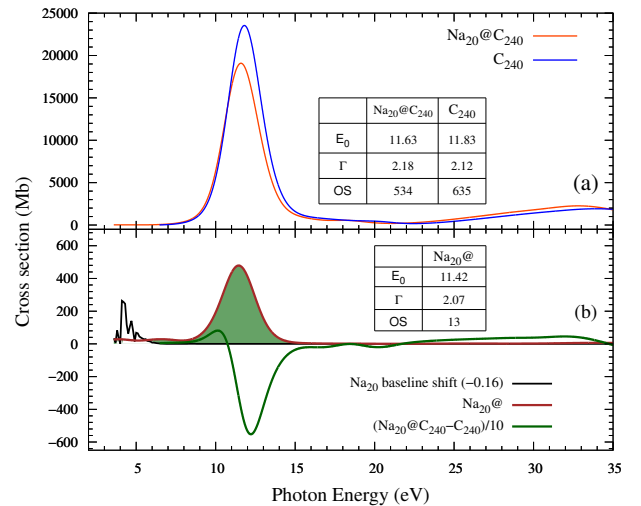


FIG. 4. (Color online) All smoothed LR-TDDFT cross section results are used. (a): The total cross sections for $\text{Na}_{20}@\text{C}_{240}$ and C_{240} are shown. The values of the fitted parameters, peak energy (E_0) and width (Γ), and oscillator strength (OS) exhausted by the GPR are given. (b): The difference (scaled-down) between $\text{Na}_{20}@\text{C}_{240}$ and C_{240} results, the raw Na_{20} result (with a slight down-shift for the aid of comparison), and the RICD plasmon feature ($\text{Na}_{20}@\text{C}_{240}$), shaded to highlight. The fitting parameters and the OS of $\text{Na}_{20}@\text{C}_{240}$ are tabulated.

results in Fig. 4(b) provides an energy-differential effect of the Na_{20} doping at GPR energies. The doping results in a slight constructive interference at lower energies but

a larger destructive interference at higher energies effecting a net reduction. This is reflected in the corresponding reduction of OS [Fig. 4(a)] utilized by the resonances. However, the value of OS spent by the ICD plasmon resonance is found to be 13 [Fig. 4(b)], which is remarkably close both to the OS (~ 15) consumed by the native plasmon resonance of Na_{20} [53] and the electron population of 14 at Na_{20} in the compound.

Making larger fullerenes is difficult. Even if achieved, the production may suffer from lower yields and higher isomer counts. However, there is a recent approach of isolating larger fullerenes from fullertube isomers [54]. Also, among various techniques [55] of synthesis and extraction of endofullerenes, the irradiation of fullerene film with metal ion beams [56] is fairly successful. This method can be extended for longer time exposure to implant multiple ions to produce clustered encapsulation. However, the technique may deplete the sample yield from film destruction. We hope that the technology will improve so the future experiments can access the current pilot prediction of plasmonic RICD.

To conclude, using a many-body framework of DFT, finely supported by a QC calculation of the ground state, we predict a hitherto unknown ICD dynamics of a plasmon resonance. It is shown that the XUV-photon driven giant plasmon of C_{240} can efficiently transfer strength *via* the resonant ICD through the ionization continuum of a sodium cluster located in the fullerene cavity. The strength of this plasmonic RICD, emerging at the otherwise mundane XUV spectrum of isolated Na_{20} , is of the same order of the cluster's native plasmon resonance, excitable only by the visible light. The study addresses calculations using a cluster-dimer in a spherical orientation. But the essence of the result should be extendable for non-spherical, even longitudinal, dimers. It may be generalized for polymers, thin films and in the liquid phase. In fact, higher wavefunction overlaps from a favorable geometry will enhance the effect. Even though experiments will be challenging at the moment, the effect predicted is fundamental, opens a new direction to push the frontier of ICD research, and promises controls in transferring large amount (in plasmonic quantities) of energy to induce remote spectroscopic events.

We thank Dr. Alexey Popov for encouraging discussions on synthesis possibilities of cluster-fullerenes for future experiments. The research is supported by the SERB, India (H.R.V), and by the US National Science Foundation Grant Nos. PHY-1806206 (H.S.C.), PHY-2110318 (H.S.C.), and CNS-1624416 (the Bartik HPC Cluster, Northwest Missouri State University). M.E.M. acknowledges the German Research Foundation DFG (FR 2833/79-1) for financial support. F.Z. acknowledges the support from DFG Research and Training Group via RTG 2247 "Quantum Mechanical Materials Modelling." M.E.M. and F.Z. also thank the computational resources at the HPC Cluster at the University of Oldenburg (Ger-

many).

* hari@iitmandi.ac.in

† himadri@nwmissouri.edu

- [1] G. Cario and J. Franck, Über Zerlegung von Wasserstoffmolekülen durch angeregte Quecksilberatome, *Zeitschrift für Physik* **11**, 161 (1922).
- [2] G.A. Jones and D.S. Bradshaw, Resonance energy transfer: from fundamental theory to recent applications, *frontiers in Physics* **7**, 100 (2019). X. Liu and J. Qiu, Recent advances in energy transfer in bulk and nanoscale luminescent materials: from spectroscopy to applications. *Chem. Soc. Rev.* **44**, 8714 (2015).
- [3] L.-Y. Hsu, W. Ding, and G.C. Schatz, Plasmon-coupled resonance energy transfer. *J. Phys. Chem. Lett.* **8**, 2357 (2017).
- [4] J. de Torres, M. Mivelle, S.B. Moparthy, H. Rigneault, N.F. Van Hulst, M.F. García-Parajó, E. Margeat, and J. Wenger, Plasmonic nanoantennas enable forbidden Förster dipole-dipole energy transfer and enhance the FRET efficiency, *Nano. Lett.* **16**, 6222 (2016).
- [5] T. Jahnke, Hergenbahn, B. Winter, R. Doörner, U. Fruhling, P.V. Demekhin, K. Gokhberg, L.S. Cederbaum, A. Ehresmann, A. Knie, and A. Dreuw, Interatomic and intermolecular Coulombic decay, *Chem. Rev.* **120**, 11295 (2020).
- [6] L.S. Cederbaum, J. Zobeley, and F. Tarantelli, Giant intermolecular decay and fragmentation of clusters, *Phys. Rev. Lett.* **79**, 4778 (1997).
- [7] T. Jahnke, A. Czasch, M.S. Schöffler, S. Schössler, A. Knapp, M.Kász, J. Titze, C. Wimmer, K. Kreidi, R.E. Grisenti, A. Staudte, O. Jagutzki, U. Hergenbahn, H. Schmidt-Böcking, and R. Dörner, Experimental observation of interatomic Coulombic decay in neon dimers, *Phys. Rev. Lett.* **93**, 163401 (2004).
- [8] K. Schnorr, A. Senftleben, M. Kurka, A. Rudenko, L. Foucar, G. Schmid, A. Broska, T. Pfeifer, K. Meyer, D. Anielski, R. Boll, D. Rolles, M. Kübel, M.F. Kling, Y.H. Jiang, S. Mondal, T. Tachibana, K. Ueda, T. Marchenko, M. Simon, G. Brenner, R. Treusch, S. Scheit, V. Averbukh, J. Ullrich, C. D. Schröter, and R. Moshhammer, Time-resolved measurement of interatomic Coulombic decay in Ne_2 , *Phys. Rev. Lett.* **111**, 093402 (2013).
- [9] S. Marburger, O. Kugeler, U. Hergenbahn, and T. Möller, Experimental evidence for interatomic Coulombic decay in Ne Clusters, *Phys. Rev. Lett.* **90**, 203401 (2003).
- [10] X. Ren, E.J. Al Maalouf, A. Dorn, and S. Denifl, Direct evidence of two interatomic relaxation mechanisms in argon dimers ionized by electron impact, *Nat. Commun.* **7**, 11093 (2016).
- [11] F. Wiegandt, F. Trinter, K. Henrichs, D. Metz, M. Pitzer, M. Waitz, E. Jabbour al Maalouf, C. Janke, J. Rist, N. Wechselberger, T. Miteva, S. Kazandjian, M. Schöffler, N. Sisourat, T. Jahnke, and R. Dörner, Direct observation of interatomic Coulombic decay and subsequent ion-atom scattering in helium nanodroplets, *Phys. Rev. A* **100**, 022707 (2019).
- [12] A.C LaForge, M. Shcherbinin, F. Stienkemeier, R. Richter, R. Moshhammer, T. Pfeifer, and M. Mudrich, Highly efficient double ionization of mixed alkali dimers

- by intermolecular Coulombic Decay, *Nat. Phys.* **2019** **15**, 247 (2019).
- [13] T. Takanashi, N.V. Golubev, C. Callegari, H. Fukuzawa, K. Motomura, D. Iablonskyi, Y. Kumagai, S. Mondal, T. Tachibana, K. Nagaya, T. Nishiyama, K. Matsunami, P. Johnsson, P. Piseri, G. Sansone, A. Dubrouil, M. Reduzzi, P. Carpeggiani, C. Vozzi, M. Devetta, M. Negro, D. Faccialà, F. Calegari, A. Trabattoni, M. C. Castrovilli, Y. Ovcharenko, M. Mudrich, F. Stienkemeier, M. Coreno, M. Alagia, B. Schütte, N. Berrah, O. Plekan, P. Finetti, C. Spezzani, E. Ferrari, E. Allaria, G. Penco, C. Serpico, G. De Ninno, B. Diviacco, S. Di Mitri, L. Giannessi, G. Jabbari, K.C. Prince, L.S. Cederbaum, Ph.V. Demekhin, A.I. Kuleff, and K. Ueda, Time-resolved measurement of interatomic Coulombic decay induced by two-photon double excitation of Ne₂, *Phys. Rev. Lett.* **118**, 033202 (2017)
- [14] F. Trinter, J.B. Williams, M. Weller, M. Waitz, M. Pitzer, J. Voigtsberger, C. Schober, G. Kastirke, C. Müller, C. Goihl, P. Burzynski, F. Wiegandt, T. Bauer, R. Wallauer, H. Sann, A. Kalinin, L. Ph. H. Schmidt, M. Schöffler, N. Sisourat, and T. Jahnke, Evolution of interatomic Coulombic decay in the time domain, *Phys. Rev. Lett.* **111**, 093401 (2013).
- [15] P. Zhang, C. Perry, T.T. Luu, D. Matselyukh, and H.J. Wörner, Intermolecular Coulombic decay in liquid water, *Phys. Rev. Lett.* **128**, 133001 (2022).
- [16] B.M. Jones, H. Hu, A. Alexandrov, W. Smith, A.E. Clark, X. Li, and T.M. Orlando, Efficient intermolecular energy exchange and soft ionization of water at nanoplatelet interfaces, *J. Phys. Chem. Lett.* **11**, 10088 (2020).
- [17] L.S. Cederbaum and A.I. Kuleff, Impact of cavity on interatomic Coulombic decay, *Nat. Commun.* **12**, 4083 (2021).
- [18] S. Barik, S. Dutta, N.R. Behera, R.K. Kushawaha, Y. Sajeew, and G. Aravind, Ambient-light-induced intermolecular Coulombic decay in unbound pyridine monomers, *Nat. Chem.* **14**, 1098 (2022).
- [19] A.C. LaForge, M. Drabbel, N.B. Brauer, M. Coreno, M. Devetta, M. Di Fraia, P. Finetti, C. Grazioli, R. Katzy, V. Lyamayev, T. Mazza, M. Mudrich, P. O’Keeffe, Y. Ovcharenko, P. Piseri, O. Plekan, K.C. Prince, R. Richter, S. Stranges, C. Callegari, T. Möller, and F. Stienkemeier, *Sci. Rep.* **4**, 3621 (2014).
- [20] D. Iablonskyi, K. Nagaya, H. Fukuzawa, K. Motomura, Y. Kumagai, S. Mondal, T. Tachibana, T. Takanashi, T. Nishiyama, K. Matsunami, P. Johnsson, P. Piseri, G. Sansone, A. Dubrouil, M. Reduzzi, P. Carpeggiani, C. Vozzi, M. Devetta, M. Negro, F. Calegari, A. Trabattoni, M.C. Castrovilli, D. Faccialà, Y. Ovcharenko, T. Möller, M. Mudrich, F. Stienkemeier, M. Coreno, M. Alagia, B. Schütte, N. Berrah, A.I. Kuleff, G. Jabbari, C. Callegari, O. Plekan, P. Finetti, C. Spezzani, E. Ferrari, E. Allaria, G. Penco, C. Serpico, G. De Ninno, I. Nikolov, B. Diviacco, S. Di Mitri, L. Giannessi, K.C. Prince, and K. Ueda, Slow Interatomic Coulombic Decay of Multiply Excited Neon Clusters, *Phys. Rev. Lett.* **117**, 276806 (2016).
- [21] J.M. Cabrera-Trujillo, J.A. Alonso, M.P. Iniguez, M.J. López, and A. Rubio, Theoretical study of the binding of Na clusters encapsulated in the C₂₄₀ fullerene, *Phys. Rev. B* **53**, 16059 (1996).
- [22] S. Yang, T. Wei, and F. Jin, When metal clusters meet carbon cages: endohedral clusterfullerenes, *Chem. Soc. Rev.* **46**, 5005 (2017).
- [23] C. Xia, C. Yin, and V.V. Kresin, Photoabsorption by volume plasmons in metal nanoclusters, *Phys. Rev. Lett.* **102**, 156802 (2009).
- [24] M.E. Madjet and H.S. Chakraborty, “Collective resonances in the photoionization of metallic nanoclusters”, *J. Phys.: Conf. Ser.* **194**, 022103 (2009).
- [25] M.A. McCune, R. De, M.E. Madjet, H.S. Chakraborty, and S.T. Manson, Plasmon-plasmon coupling in nested fullerenes: photoexcitation of interlayer plasmonic cross modes, *J. Phys. B* **44**, 241002 (2011).
- [26] M.H. Javani, J.B. Wise, R. De, M.E. Madjet, S.T. Manson, and H.S. Chakraborty, Resonant Auger–intersite-Coulombic hybridized decay in the photoionization of endohedral fullerenes, *Phys. Rev. A* **89**, 063420 (2014).
- [27] M. Magrakvelidze, R. De, M.H. Javani, M.E. Madjet, S.T. Manson, and H.S. Chakraborty, Coherence of Auger and inter-Coulombic decay processes in the photoionization of Ar@C₆₀ versus Kr@C₆₀, *Eur. Phys. J. D* **70**, 96 (2016).
- [28] R. De, M. Magrakvelidze, M.E. Madjet, S.T. Manson, and H.S. Chakraborty, First prediction of inter-Coulombic decay of C₆₀ inner vacancies through the continuum of confined atoms, *J. Phys. B* **49**, 11LT01 (2016).
- [29] M. Khokhlova, L. Bahmanpour, N. Bachhawat, B. Cooper, and V. Averbukh, Interatomic coulombic decay rate in endohedral complexes, *J. Phys. B* **53**, 184002 (2021).
- [30] R. De, E. Ali, S.T. Manson, and H.S. Chakraborty, Density functional study of the variants of inter-Coulombic decay resonances in the photoionization of Cl@C₆₀, *Phys. Scr.* **96**, 104007 (2021).
- [31] R. Obaid, H. Xiong, S. Augustin, K. Schnorr, U. Ablikim, A. Battistoni, T.J.A. Wolf, R.C. Bilodeau, T. Osipov, K. Gokhberg, D. Rolles, A.C. LaForge, and N. Berrah, Intermolecular Coulombic decay in endohedral fullerene at the $4d \rightarrow 4f$ Resonance, *Phys. Rev. Lett.* **124**, 113002 (2020).
- [32] See Supplemental Material [url] for details of the methodology which includes Refs. [33]–[45].
- [33] TURBOMOLE V7.5 2020, a development of University of Karlsruhe and Forschungszentrum Karlsruhe GmbH, 1989–2007, TURBOMOLE GmbH, since 2007; available from <http://www.turbomole.com>.
- [34] A. Becke, Density-functional thermochemistry. III. The role of exact exchange, *J. Chem. Phys.* **98**, 5648 (1993).
- [35] P.J. Stephens, F.J. Devlin, C.F. Chabalowski, and M.J. Frisch, Ab initio calculation of vibrational absorption and circular-dichroism spectra using density functional force fields. *J. Phys. Chem.* **98**, 11623 (1994).
- [36] S. Grimme, J. Antony, S. Ehrlich, and H. Krieg, A consistent and accurate ab initio parametrization of density functional dispersion correction (DFT-D) for the 94 elements H–Pu, *J. Chem. Phys.* **132**, 154104 (2010).
- [37] F. Weigend and R. Ahlrichs, Balanced basis sets of split valence, triple zeta valence and quadruple zeta valence quality for H to Rn: Design and assessment of accuracy, *Phys. Chem Chem. Phys.* **7**, 3297 (2005).
- [38] J. Choi, E.H. Chang, D.M. Anstine, M.E. Madjet, and H.S. Chakraborty, Effects of exchange-correlation potentials on the density-functional description of C₆₀ versus C₂₄₀, *Phys. Rev. A* **95**, 023404 (2017).
- [39] R. Shaik, H.R. Varma, and H.S. Chakraborty, Exchange-correlation functional in density-functional description of

- the photoionization of Na clusters, *in preparation*.
- [40] O. Gunnarsson and B. Lundqvist, Exchange and correlation in atoms, molecules, and solids by the spin-density-functional formalism, *Phys. Rev. B* **13**, 4274 (1976).
- [41] J. P. Perdew and Alex Zunger, Self-interaction correction to density-functional approximations for many-electron systems, *Phys. Rev. B* **23**, 5048 (1981).
- [42] G. L. Oliver and J. P. Perdew, Spin-density gradient expansion for the kinetic energy, *Phys. Rev. A* **20**, 397 (1979).
- [43] M. Petersilka, U.J. Gossmann and E.K.U. Gross, Excitation energies from time-dependent density-functional theory, *Phys. Rev. Lett.* **76**, 1212 (1996).
- [44] P.J. Feibelman, Microscopic calculation of electromagnetic fields in refraction at a jellium–vacuum interface, *Phys. Rev. B* **12**, 1319 (1975).
- [45] G. Bertsch, An RPA program for jellium spheres, *Comput. Phys. Commun.* **60**, 247 (1990).
- [46] A. Rüdél, R. Hentges, U. Becker, H.S. Chakraborty, M.E. Madjet, and J.M. Rost, Imaging Delocalized Electron Clouds: Photoionization of C_{240} in Fourier Reciprocal Space, *Phys. Rev. Lett.* **89**, 125503 (2002).
- [47] S.W.J. Scully, E.D. Emmons, M.F. Gharaibeh, R.A. Phaneuf, A.L.D. Kilcoyne, A.S. Schlachter, S. Schippers, A. Müller, H.S. Chakraborty, M.E. Madjet, and J.M. Rost, Photoexcitation of a volume plasmon in C_{60} Ions, *Phys. Rev. Lett.* **94**, 065503 (2005).
- [48] A. Zangwill and P. Soven, *Phys. Rev. A* **21**, 1561 (1980).
- [49] M.E. Madjet, H.S. Chakraborty, J.M. Rost, and S.T. Manson, Photoionization of C_{60} : a model study, *J. Phys. B* **41**, 105101 (2008).
- [50] S. Biswas, A. Trabatttoni, P. Rupp, M. Magrakvelidze, M.E. Madjet, U. De Giovannini, M.C. Castrovilli, M. Galli, Q. Liu, E.P. Månsson, J. Schötz, V. Wanie, F. Légaré, P. Wnuk, M. Nisoli, A. Rubio, H.S. Chakraborty, M.F. Kling, F. Calegari, Attosecond correlated electron dynamics at C_{60} giant plasmon resonance, (2022) <http://arxiv.org/abs/2111.14464>.
- [51] U. Fano, Effects of configuration interaction on intensities and phase shifts, *Phys. Rev.* **124**, 1866 (1961).
- [52] G. Basnayake, Y. Ranathunga, S.K Lee, and W. Li, Three-dimensional (3D) velocity map imaging: from technique to application, *J. Phys. B*, **55**, 023001 (2022).
- [53] R. Shaik, H.R. Varma, and H.S. Chakraborty, Collective effects in photoionization of sodium clusters: plasmon resonance spill, induced attractive force and correlation minimum, *J. Phys. B* **54**, 125101 (2021).
- [54] R.M. Koenig, H.-R. Tian, T.L. Seeler, K.R. Tepper, H.M. Franklin, Z.-C. Chen, S.-Y. Xie, and S. Stevenson, Fullertubes: cylindrical carbon with half-fullerene end-caps and tubular graphene belts, their chemical enrichment, crystallography of pristine C_{90} - $D_{5h}(1)$ and C_{100} - $D_{5d}(1)$ fullertubes, and isolation of C_{108} , C_{120} , C_{132} , and C_{156} cages of unknown structures, *J. Am. Chem. Soc.* **142**, 15614 (2020).
- [55] A.A. Popov, Synthesis and molecular structures of endohedral fullerenes, *Endohedral Fullerenes: Electron Transfer and Spin*, Nanostructure Science and Technology Series, ed: A.A. Popov, Springer, Cham (2017).
- [56] C.Y. Lee, Ti^+ and Mg^+ Ion beam extraction from the modified bernas ion source, *J. Korean Phys. Soc.* **76**, 638 (2020).